geosciences

Article

Natural Hazard Assessment in Western Saudi Arabia using Remote Sensing and GIS Methods

Barbara Theilen-Willige [1], and Helmut Wenzel [2]

[1] Technische Universität Berlin (TU Berlin), Institute of Applied Geosciences, Sekr. BH 3-2, Ernst Reuter-Platz 1, D-10587 Berlin, Germany; Barbara.Theilen-Willige@t-online.de

[2] Wenzel Consulting Engineers GmbH, Hofstattgasse 22-21, 1180 Vienna, Austria; helmut.wenzel@wenzel-consult.com

* Correspondence: Barbara.Theilen-Willige@t-online.de

Received: date; Accepted: date; Published: date

Abstract: The most frequent disasters in Western Saudi Arabia are flash floods, earthquakes and volcanism, especially submarine volcanism potentially causing tsunamis in the Red Sea and submarine mass movements, dust storms and droughts. As the consequences and effects of the climate change are expected to have an increasing impact on the intensity and occurrence of geohazards as flash floods, length of drought periods, or dust storms, the systematic, continuous monitoring of these hazards and affected areas using satellite data and integration of the results into a GIS data base is an important issue for hazard preparedness. Visual interpretation and digital image processing of optical aerial and satellite images as well as radar images, combined with ASTER, SRTM and ALOS PALSAR DEM data are used for the mapping and inventory of areas prone to geohazards due to their geomorphologic and geologic disposition. Causal or critical environmental factors influencing the disposition to be affected by hazards can be analyzed interactively, then, in a GIS database. How remote sensing and GIS methods can contribute to the detection and continuously monitoring of geohazards in Western Saudi Arabia is demonstrated by several examples: Detection of areas prone to hydrological hazards such as flash floods causing flooding of roads and settlements, tracing of dust storms, outlining of coastal areas of the Red Sea prone to tsunami flooding and storm surge, mapping of traces of recent volcanic activity, and of fault / fracture zones and structural features.

Keywords: W-Saudi Arabia; natural hazards; remote sensing; GIS

1. Introduction

Western Saudi Arabia is prone to different natural hazards such as earthquakes, tsunamis and volcanic hazards, as well as flash floods after heavy rainfalls. Slope failure, especially rock fall, is a common phenomenon in the mountainous regions. Shifting sand dunes and dust storms are a serious natural hazard being faced [1]. Over the last decades, floods have been the most recurrent disasters recorded in the International Disaster Database EM-DAT [2], followed by earthquakes, storms and droughts, indicating a strong need for early warning systems. The low percentage for droughts listed in the EM-DAT is due to limited data availability [3].

As the consequences and effects of the climate change will have an increasing impact on the intensity and occurrence of natural hazards such as flash floods, length of drought periods, or storms [4], the surveillance and systematic, continuous monitoring of these hazards is an important issue of this research.

Further on the human impact in the landscape has to be considered (increasing of built areas, mining, more intensified land use). The increase of the built environment and the enlargement of urban areas has led to a great impact on the landscape and susceptibility to natural hazards.

An inventory of past geohazards is one of the main prerequisites for an objective hazard assessment, which includes both the spatial and the temporal aspects of the probability of natural hazard occurrence. Such an objective hazard assessment requires a multi-source, systematic record including regular documentation of temporal information on occurrence that cannot be derived from a historical inventory alone. The ability to undertake the assessment, monitoring and modeling can be improved to a considerable extent through the current advances in remote sensing and GIS technology. This is demonstrated in the scope of this study by the following examples:

- Flooding: Detection of areas prone to flash floods
- Seismic hazards: Mapping of fault and fracture zones and of structural features (that might be of influence on seismic hazards) based on remote sensing data
- Volcanism: Inventory of volcanic features
- Tsunami hazards: Detection of areas prone to tsunami flooding

2. Natural Hazards

2.1. Flash Floods

In the arid areas of western Saudi Arabia flash floods are generated after high-intensity rainfall events, particularly on steep mountainous terrain and hilly slopes that are barren and lack vegetation cover. Flash floods and associated debris flows are quite common along the steeper slopes and valleys of the western escarpments [5] during the wetter season. The runoff generated during the occasional heavy rainstorms in the region, coupled with the urban growth are the main causes of the occurrence of flash floods. Though the average annual rainfall in Saudi Arabia is only about 100 mm, hydro-logical hazards occur especially in the big cities like Jeddah and Makkah mainly due to rapid urbanization which has led to the development of housing in topographically low-lying regions and obstruction of the natural drainage systems. The urbanization significantly decreases the permeability of the soil and, thus, leads to a crucial increase in hazardous water surface runoff [6].

2.2. Earthquake Hazard

The general physiography of western Saudi Arabia is characterized by the Red Sea coastal plains and the escarpment foothills called Tihama. Along this zone, sabkha areas exist in longitudinal stretches parallel to the shore line of the Red Sea [5]. The Arabian Peninsula forms a tectonic plate surrounded by active boundaries with earthquake occurrence [7]. Following the rifting of the Red Sea Basin some 30 million years ago, the Red Sea region became a broad zone of active deformation between Africa and Arabia. Seismicity in the region is caused by the collision of the Arabian plate with the Eurasian plate along the Zagros and Bitlis thrust system, rifting and sea floor spreading in the Red Sea and Gulf of Aden. A concentration of earthquake activities is monitored along the Red Sea Rift and the Gulf of Aqaba [1], [8].

The Red Sea is a narrow ocean basin, separating the African plate from Arabian plate. It is approximately 3000 km long and about 100 to 300 km wide. The margins of the Red Sea are forming steep fault scarps, that rise sharply from the coast. In the central and southern Red Sea, the rifting area is characterized in the median valley with an axial trough that reaches water depths of more than 2000 m, and by a basaltic oceanic crust with magnetic anomalies [9]. Most of the earthquakes occur within the spreading zone in the rift valley region, which is characterized by continuous sea floor spreading [8], see Figure 1. Earthquake activities are oriented along major faults or clustered in certain spots [10]. Concentrations of earthquake activity are seen where the spreading zone is intersected by the NE-SW striking transform faults [11]. A great part of the seismicity of in western Saudi Arabia is volcanic-related and, thus, more of the swarm type.

When researching seismic and aseismic activity and the geodynamic, plate tectonic related, active movements in Western Saudi Arabia, the focus is directed towards the monitoring of larger fault zones, especially active fault zones and active shear zones. Understanding active tectonic processes has become fundamental not only for the detection of areas prone to earthquakes, but also for the monitoring of infrastructure (bridges, tunnels and pipelines).

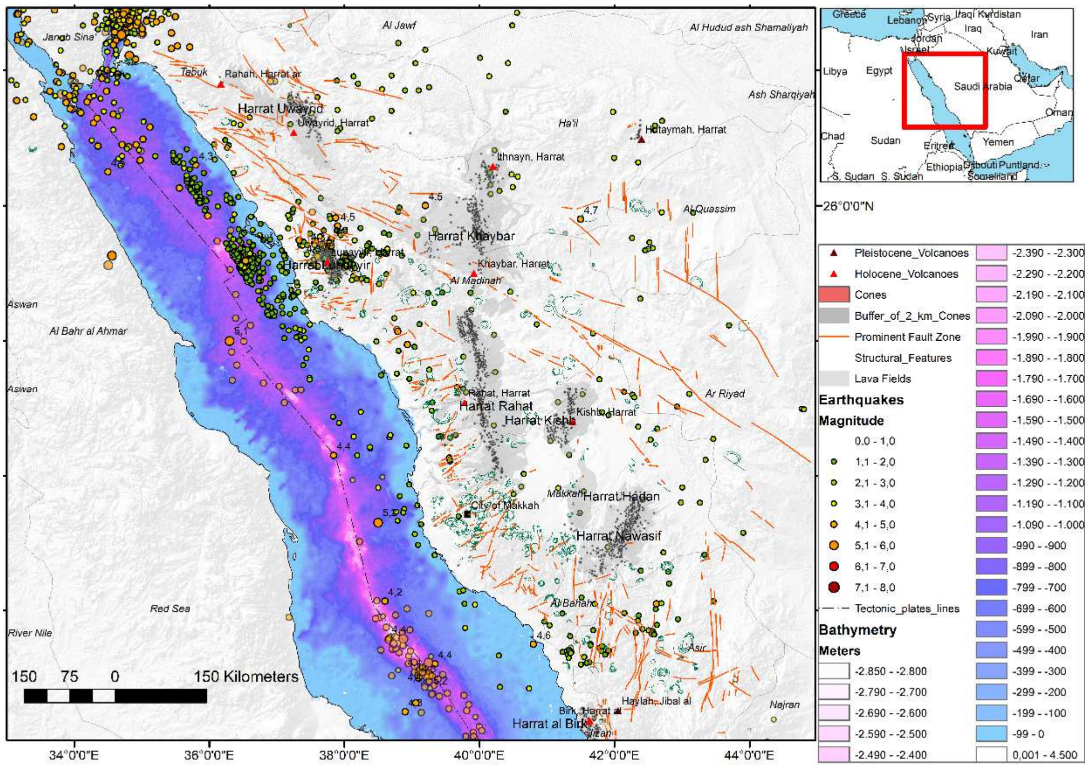

Figure 1. Earthquakes in West-Saudi Arabia (Earthquake data: USGS, ISC, EMSC) [12,13,14] during the last decades (sources: lava shapefile from USGS, Pleistocene and Holocene volcano shapefiles from Smithsonian Institution's Global Volcanism Program (GVP) [15], cinder cones and larger lineaments (red lines) mapped based on satellite data)

2.3. Volcanic Hazards

The western Arabian plate encompasses at least 15 continental, intraplate volcanic fields, known in Arabic as Harrat (Figure 1). The first period of volcanism (30–15 Ma) was associated with the doming and rifting of the Proterozoic basement of the present Arabian Nubian Shield along the north-northwest trending rift system leading to the opening of the Red Sea basin. The second period of volcanism (< 12 Ma) is characterized by north–south trending vent system associated with the onset of a new north–south trending 900 km long crustal rift system passing through the 600 km long Makkah-Madinah volcanic line. Individual volcanic fields can be very large, such as Harrat Ash Shams and Harrat Rahat. Harrat Al Madinah volcanic province (a part of Harrat Rahat) is an active volcanic field characterized by two historical eruptions, one in 641AD and another in 1256 AD [16]. These volcanic fields are forming a broad zone sub-parallel to the Red Sea Rift. Hawaiian to Strombolian type eruptions created lava spatter, shield volcanos and scoria cones.

Northwestern Saudi Arabia experienced notable earthquake swarms during April–June 2009. These earthquakes took place beneath Harrat Lunayyir [17]. The maximum magnitude recorded was 5.4, and this earthquake caused minor structural damage in the town of Al-Eis about 40 km from the city of Madinah [17]. As a result of this earthquake, a northwest trending 8-km-long surface rupture propagated across the northern part of the volcanic field. Harrat Lunayyir is one of the smallest and youngest of the extensive volcanic fields on the western Arabian Peninsula, lying ~ 60 km east of the Red Sea and covering a surface area of ~3500 km² [18]). Historical records of volcanic activity indicate that over 20 eruptions have occurred on the Arabian Peninsula during the past 2000 years [19], including one possible eruption in Harrat Lunayyir about 1000 years ago, recent dyke intrusions monitored in 2009 [18].

2.4. Tsunami Hazards

The potential of magmatic and volcanic activity to move large volumes of submarine materials like lava or turbidity currents that could eventually originate water mass movements has to be taken into account in the Red Sea. The capacity of submarine seismic activity (earthquakes) to produce tsunamis in the Red Sea is known [20]. The Arabian Peninsula has been affected by tsunamis in the past, see Figure 2. Submarine, volcanic eruptions can produce volcanic tremors, earthquakes, and sudden submarine displacement of rocks and sediments, originated either by movement of magma masses under the sea-surface, formation of fractures, effusion of lava flows, or sudden formation of islands.

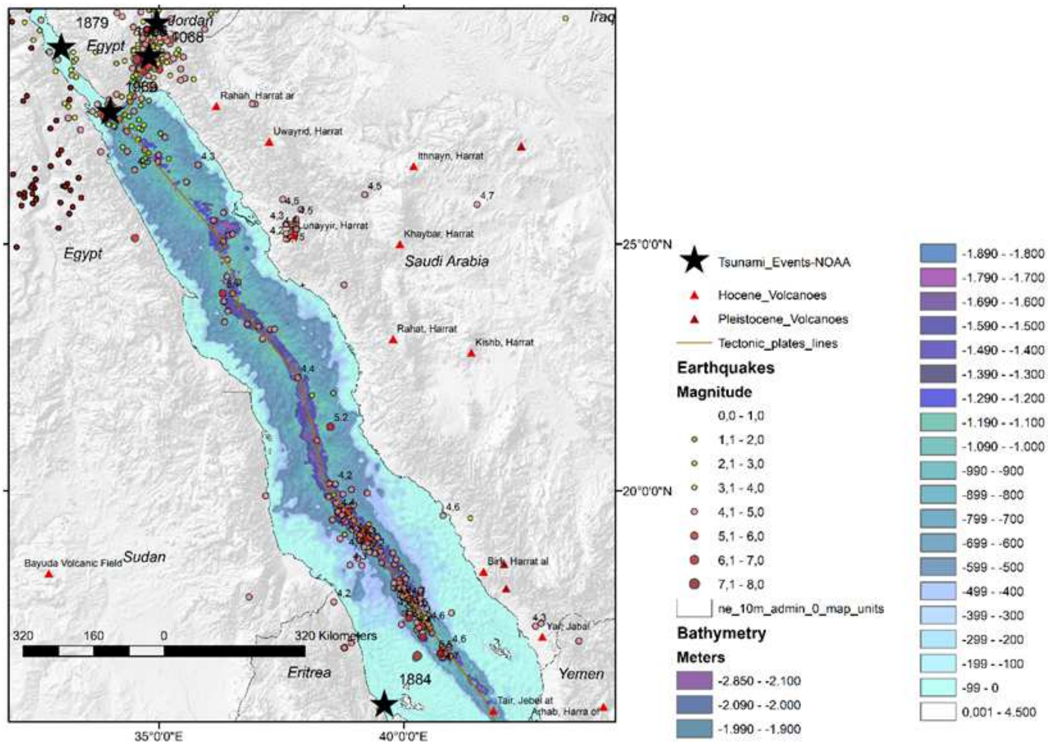

Figure 2. Tsunami events (blue stars) in the Red Sea as documented by NOAA [21]
Bathymetric data: GEBCO [22]

With an elongate shape (width of up to 355 km and a length of 2250 km) the prerequisite for seiche development in the Red Sea is given. Seiches are typically caused when strong winds and rapid changes in atmospheric pressure push water from one side of the Red Sea to the other. When the wind stops, the water rebounds to the other side of the enclosed area [23]. The water then can continue to oscillate back and forth for hours or even days. Winds and atmospheric pressure can contribute to the formation of both, seiches and meteo-tsunamis; however, winds are typically more important to a seiche motion, while pressure often plays a substantial role in meteo-tsunami formation (NOAA).

3. Materials and Methods

The interdisciplinary approach used in the scope of this research comprises remote sensing data, climate data, geological, geophysical and geomorphological / topographic data and GIS methods. The processing and analysis of Landsat and Aster images of Western Saudi Arabia that have been available for decades, will support the detection of environmental changes. GeoInformation Systems (GIS), used together with remote sensing data and field research, contribute to the analysis and presentation of information related to the geo-hazards in the investigation area. The interactions and dependencies between different causal and preparatory factors influencing the susceptibility to natural hazards can be visualized and weighted step by step in this GIS environment [24, 25].

Different satellite data and image processing tools were tested in order to find out how far the satellite data can contribute to the detection of causal factors influencing the susceptibility of Western Saudi Arabia to natural hazards due to the geomorphologic disposition of the region such as to flash floods and to slope failure. For the present study Landsat-,ASTER, Sentinel-2 and OrbView images are available [26]. The use of multi-temporal satellite remote sensing data opens up the opportunity for the development of efficient methods for systematic spatio-temporal mapping over large areas. For a better overview of seasonal influences on natural hazards a multi-temporal analysis of different satellite data was carried out. A comparative analysis of optical satellite data and the Sentinel and ALOS PALSAR radar data provided by the Alaska Satellite Facility [27] was carried out, in order to derive more structural geologic information. Due to the geomorphologic situation causing distortion of the radar signals in this area, the evaluation of Sentinel 1 A and B provided by ESA and PALSAR radar images requires geometric correction and calibration. Radar related layover-effects and foreshortening effects are limiting factors in this partly mountainous environment. The processing of the radar data was carried out using the SNAP software of ESA.

Satellite imageries and DEM data are used for generating an image based GIS data base and combined with different geodata and other thematic maps. This database comprises two main parts: (a) the datasets with the background geographic conditions and (b) the hazard inventory dataset. The integration of seismic records, geomorphologic analysis, digital elevation data, lithology, land cover and suitable high-resolution remote sensing data are part of this data mining. In the scope of this study, open-source data as provided by OpenStreetMap [28] or Google Earth were used in addition for gaining the necessary information, as well as evaluations of ESRI base maps and further ArcGIS-Online-tools and data.

One of the first steps towards the assessment of the different geohazards is the susceptibility analysis and mapping. The susceptibility analysis and maps comprise the potential location of the hazard source. Such susceptibility maps are a valuable tool for assessing current and potential risks that can be used as input for developing early warning systems and mitigation plans, such as selecting the most suitable locations for construction of structures and roads. According to the resulting susceptibility maps, hot spots can be identified where more detailed analysis should follow. Detailed information on historic records of both occurrences and event data are necessary for the hazard analysis.

4. Evaluation Results

4.1. Combined evaluations of optical satellite images and satellite radar data for the detection of areas prone to flash floods

Satellite images can contribute to the detection of areas prone to flash floods when acquired during or shortly after the flash flood events. Cloud covers are often a hindrance. Therefore radar data are a valuable, additional tool for identifying flooded areas. They help not only to detect areas affected by flooding, but also to visualize the related sediment flow and disposition. The monitoring and mapping of flash flood sediments and erosion pattern is an important issue for the planning of settlements, infrastructure and supply lines. Figure 3 shows a Sentinel 2 (RGB band combination of Band 8, 4 and 2) and a Sentinel 1-radar scene from an area west of the city of Mecca. Traces of sediment transport of flash floods can be easily detected on the optical satellite data of Sentinel 2 in blue colors.

The differences in brightness between pixels in the radar image, marked by changes in the gray scale and backscatter intensity due to surface roughness changes contribute to the detection of sediment properties. Dark image tones are associated with finer grained sediment sheets (clay, sand) because the incident radar signals were largely reflected from their “radar-smooth” surfaces in a mirror-like fashion away from the satellite antenna. Coarse-grained sediments appear in lighter tones as their more radar-rough surfaces generate a diffuse and stronger signal return / radar backscatter (Figure 3). As the distance to the source areas of the transported sediments during a flash flood is relatively short in this area, coarse-grained, loose gravel seems to be prevailing, thus, causing the brighter tones on the radar image (diffuse radar backscatter). The finer grained material is transported to the larger valley towards the coastal area, where it is affected by aeolian activity forming dune fields.

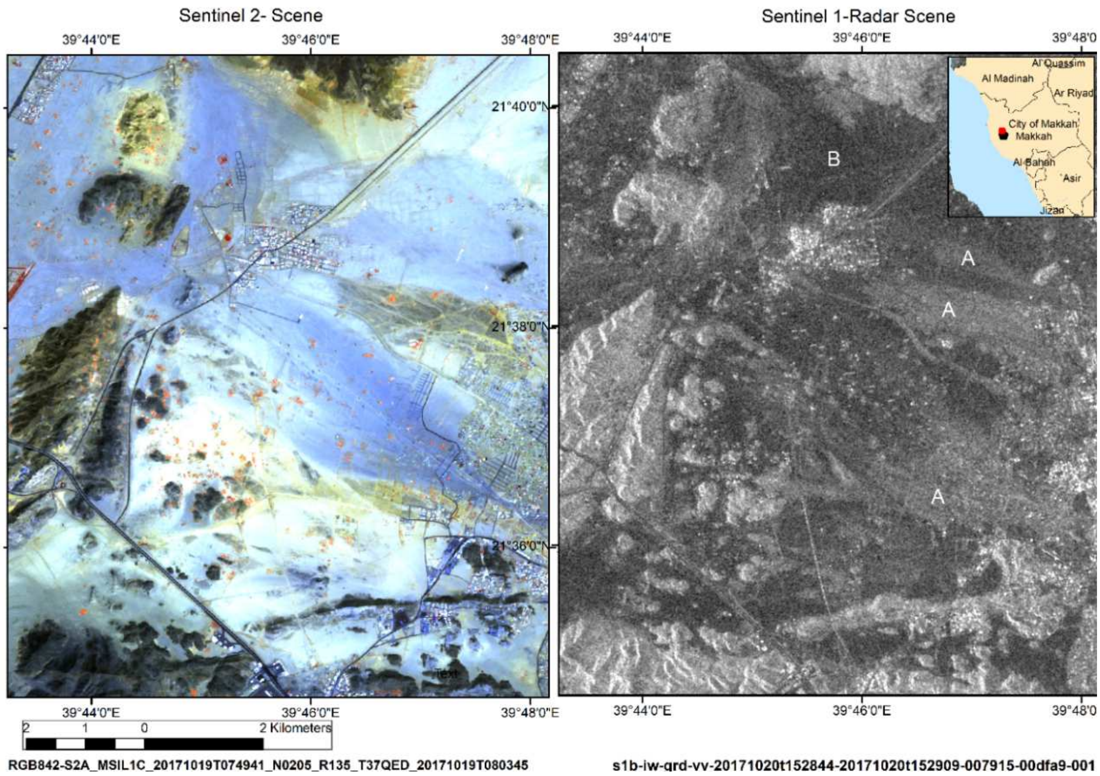

Figure 3. Sediment (blue colors) after heavy rains visible on a Sentinel 2-scene (acquisition date: 19.10.2017) and on the Sentinel 1 radar scene (acquisition date: 20.10.2017) west of the City of Mecca, A – coarser-grained sediments, B – finer grained sediments

4.2. Evaluation of Digital Elevation Model (DEM) Data

A weighted overlay procedure can be carried out for the detection of areas with higher susceptibility to flash floods by extracting causal / preparatory factors and, then, by aggregating these factors in the weighted overlay-tool of ArcGIS [25]. The susceptibility model represents a methodological approach to facilitate the spatial identification of flood zones. This approach is used to get information of areas that are susceptible to flash floods due to their morphometric disposition. Flash floods occur predominantly in basin / depression-areas showing slope angles < 5 °, terrain curvature = 0, high flow accumulation and drop flow according to the drop raster calculation in ArcGIS and the lowest, local height level (Figure 4). Whenever the before mentioned, causal factors occur aggregated in an area, the susceptibility to flooding is rising. Areas with these morphometric properties are susceptible to flash floods during heavy rain fall and to higher infiltration of the surface water.

As the urban development has led to the expansion of the built area into those broader valleys and basins, these areas will be exposed to flash floods after heavy rains.

4.3. Structural, tectonic analysis of satellite images as contribution to seismic research

The GIS integrated, structural evaluation of remote sensing data contributes to the detection of a) larger, prominent fault zones, of (b) traces of structural features such as ring structures or folds and(c) of traces of compression at the border zones of the Red Sea due to the rifting processes.

(a) The structural / geologic evaluation of optical satellite images and of radar data allows a quite

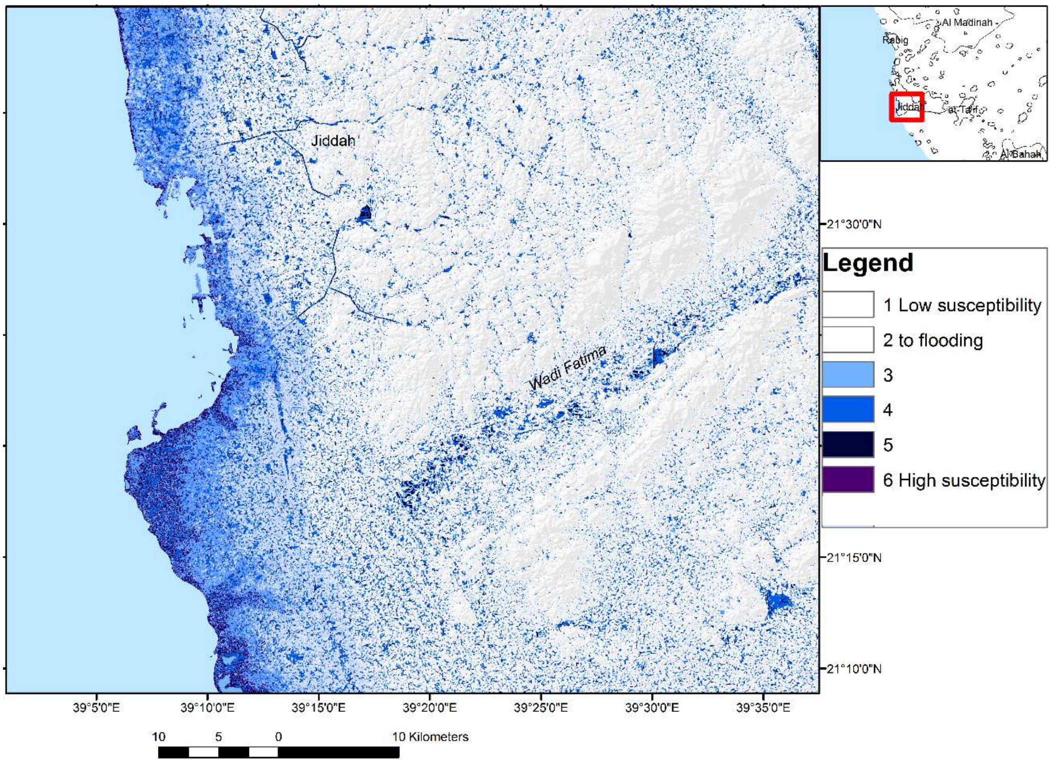

Figure 4. Weighted overlay of morphometric factors influencing the susceptibility to flooding by flash floods in the area of Jiddah, factors: curvature = 0, slope degree < 10°, height level < 10 m, dropraster < 100.000 (calculated in ArcGIS), flow accumulation > 5000

precise mapping of larger fault zones. Existing fault zones not only play an important role for ongoing tectonic processes, but also for uprising magma. They form zones of weakness that can form an entrance for the intrusion of magmatic bodies. Especially earthquake swarms were related in the past to magmatic activity [17]. Therefore, the different satellite images were used, especially to detect traces of neotectonic movements in the youngest outcrops of rocks and sediments. Whereas the oldest Precambrian / Cambrian rocks show evidence of many stress imprints in the scope of earth geologic history, the youngest strata provide hints of the more actual geodynamic processes. Therefore, the Quaternary sediments and volcanic strata were investigated as well, whether traces of younger faults can be detected. Whenever distinct linear traces of fault zones and shear zones (such as scarps and valleys cutting through older lithologic units) are visible on the satellite images, there is a hint related to active faults. The Principal Component analysis (PCA) of Landsat data helps to identify larger, prominent fault zones (Figure 5).

(b) Another important aspect is the detection of circular structures in the Precambrian and Cambrian rocks, even when deeply eroded and only visible on the satellite images because of the circular outline. The annular structures show circular or oval shapes and they are different, in their structures, from other surrounding geologic phenomena, most of them consisting of intrusive batholiths [29]. Also, these structures differ in their dimensions, origin and the characteristics of their identification on satellite images. Some form prominent domes, others are only visible due to circular, tonal anomalies in the sedimentary covers. Their dimensions range from many meters till hundreds of meters up to more than 100 kms. The majority of these circular structures with 10 to 25 km in diameter were generally created by Precambrian intrusive, magmatic bodies of different composition (mainly granitc) and geomechanic properties.

The knowledge of the position of circular structures plays an important role when dealing with seismic and aseismic movements in this area. The earthquake pattern might be influenced by the circular structures as well as the recent volcanic activity. It seems as if the larger fault zones are "bending" around the structures. For a better understanding of the geomechanic processes in this area (movements towards northeast with velocities of 10 to 15 mm / year [30], it has to be considered that the intrusive bodies might react mechanically different than the surrounding rocks, potentially forming asperities that could lead to earthquakes in case of stress accumulation. Ring structures with their different, geomechanical properties, especially when occurring block-wise, form a relatively stable "hindrance" against tectonic movements.

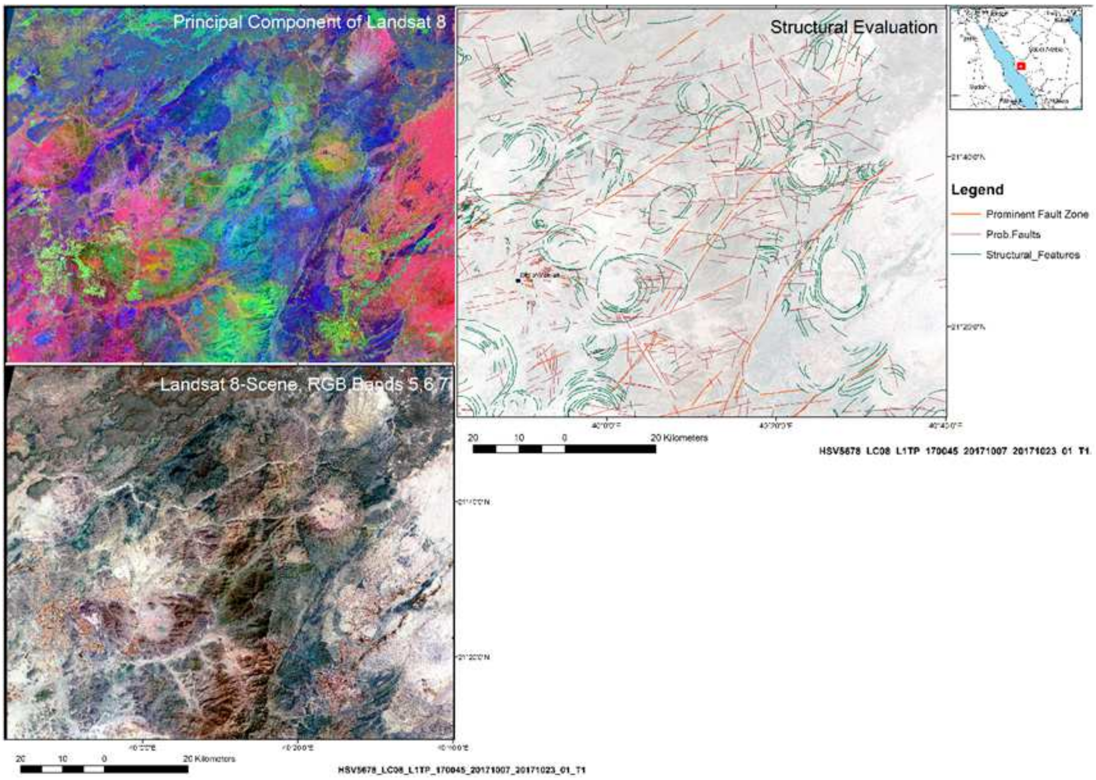

Figure 5. Image processing and structural evaluation for the detection of prominent fault zones and circular features

PCA is a linear transformation that reorganizes the variance in a multiband image into a new set of image bands. These PC bands are uncorrelated linear combinations of the input bands. A PC transform finds a new set of orthogonal axes with their origin at the data mean, and it rotates them so the data variance is maximized (ESRI Online Help in ArcGIS)

During the last decades only few earthquakes were documented within the area of the circular structures. In case of stronger earthquakes, even far-field ones, these circular structures could influence seismic wave propagation and would cause lateral variations in seismic wave speeds. Especially the thermal bands of ASTER and Landsat 8 and Sentinel 1 radar images allow the detection of circular structures that often cannot be detected in the field easily due to sedimentary covers. Due to the penetration capabilities of Sentinel 1- C-Band radar into unconsolidated sedimentary covers up to several dm subsurface structures become visible that often remain partly undetected on optical satellite images. The satellite radar images of this arid area clearly reveal penetration of the radar signals through covers of eolian and flash flood /fluvial deposits. Penetration of the masking sand covers facilitates the detection of the underlying surface due to the reflection at the sand / bedrock interface. Dark image tones are associated with deeper sand sheets because the incident radar signals were largely reflected from their "radar-smooth" surfaces in a mirror-like fashion away from the satellite antenna. The granitic rocks and gneisses appear in lighter tones as their more radar-rough surfaces cause a diffuse and stronger signal return / radar backscatter. The ring structure shown in Figure 6 appears even more detailed on the radar scene (Fig.6, image 4) due to the subtle differences in the radar reflection. Thus, satellite data help considerably to a systematic inventory of ring structures.

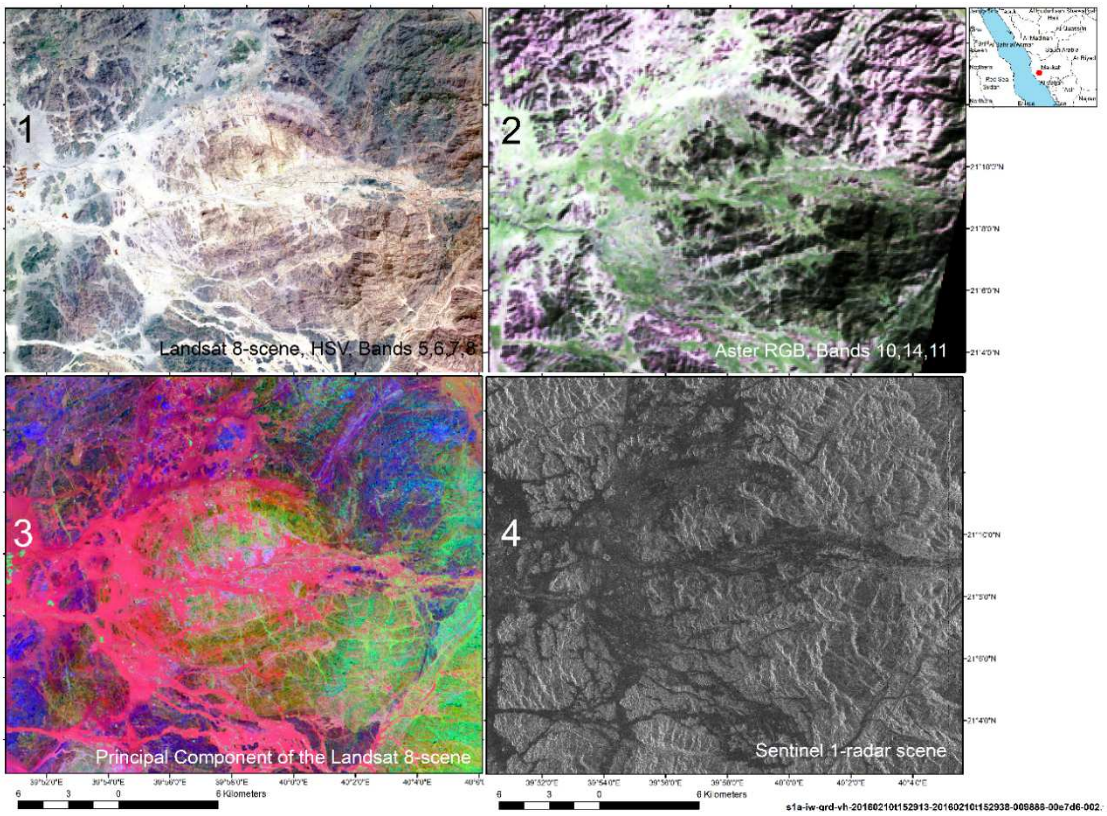

Figure 6. Use of different satellite data for providing structural information of a circular structure in the south of Makkah
1 - Landsat 8, HSV, Bands 5,6,7,8_LC08_L1TP_170045_20171007_20171023_01_T1
2 - ASTER, RGB, Bands 10,14,11-AST_L1T_00301032018080650_20180104121027_17567
3 – Principal Component (PC) of the Landsat 8-data
4 – Sentinel 1-radar image, s1a-iw-grd-vh-20160210t152913-20160210t152938-009886-00e7d6-002

(c) The coast-near areas clearly show evidence of linear features oriented NW-SE to NNW-SSE parallel to the axis of the Red Sea rift valley (Figure 7). As the area is moving towards NE, theses curvi-linear features might be related to traces of compression due to accretionary thrusting and thrust-related structures. The striking direction of the assumed traces of compression changes in close relation, parallel to the orientation of the rifting axis from NW-SE to NNW-SSE. SW-NE oriented, linear elements, perpendicular to the rift valley main axis, are very prominent on the satellite images as well. Of course, there is a need to verify these features in the field. These linear features could be partly correlated with known larger shear zones such as the Wadi Fatima shear zone [31]. Examples of the visibility of these traces are shown in the next figures (Figures 8-10).

Linear tonal anomalies and linear morphologic features help to detect larger fault zones on radar images. The differences in brightness between pixels in the Sentinel-1 radar image (Figure 10), marked by changes in the gray scale and backscatter intensity due to surface roughness changes contribute to the location of fault zones. The illumination geometry of the radar signals from west supports the detection of fault zones parallel to the rift zone.

Traces of probable compression can be visualized as well by processing of DEM data in order to enhance linear depressions and ridges oriented perpendicular to the main stress field. A digital map of depressions can be obtained by the map algebra operation of subtracting the depression-free DEM from the original DEM: (Fill-Aster-Mosaic) - (Aster-Mosaic) or the Sink-Tool in ArcGIS. The methodology is a semi-automatic approach involving several steps: (a) DEM acquisition and (b) sink-depth calculation using the difference between the raw DEM and the corresponding DEM with sinks filled.

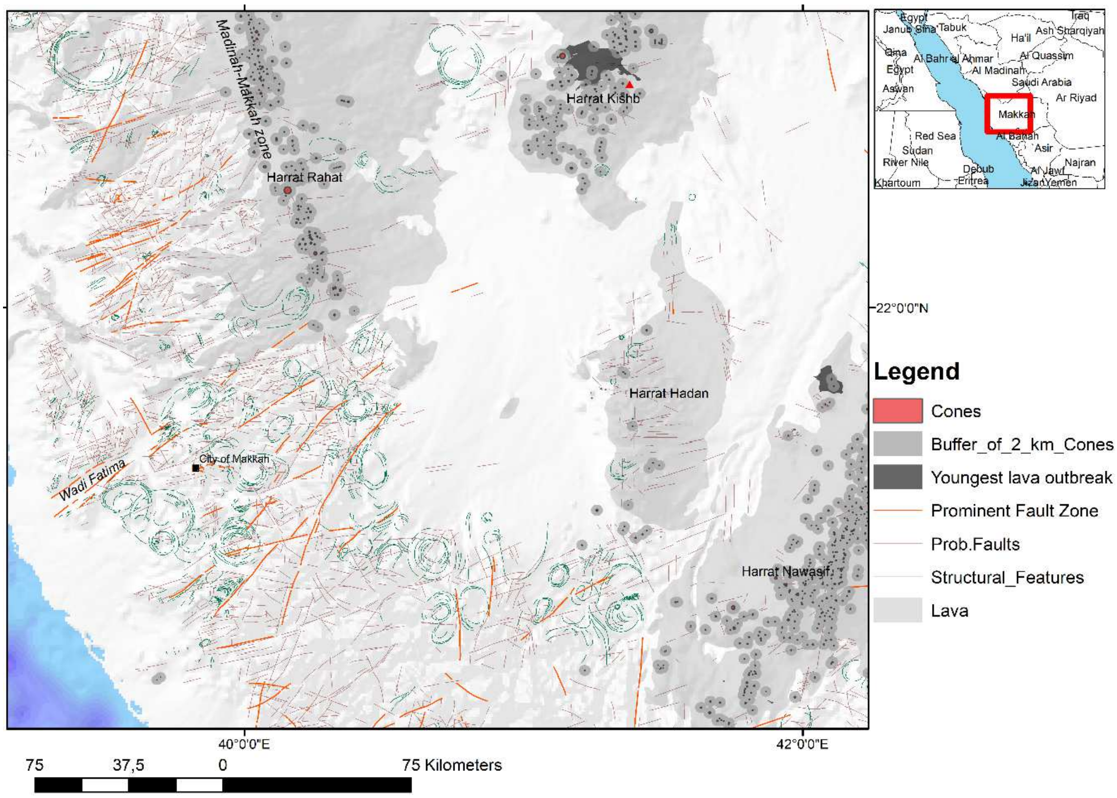

Figure 7. Larger, prominent lineaments, ring structures and volcanic features mapped based on different satellite data

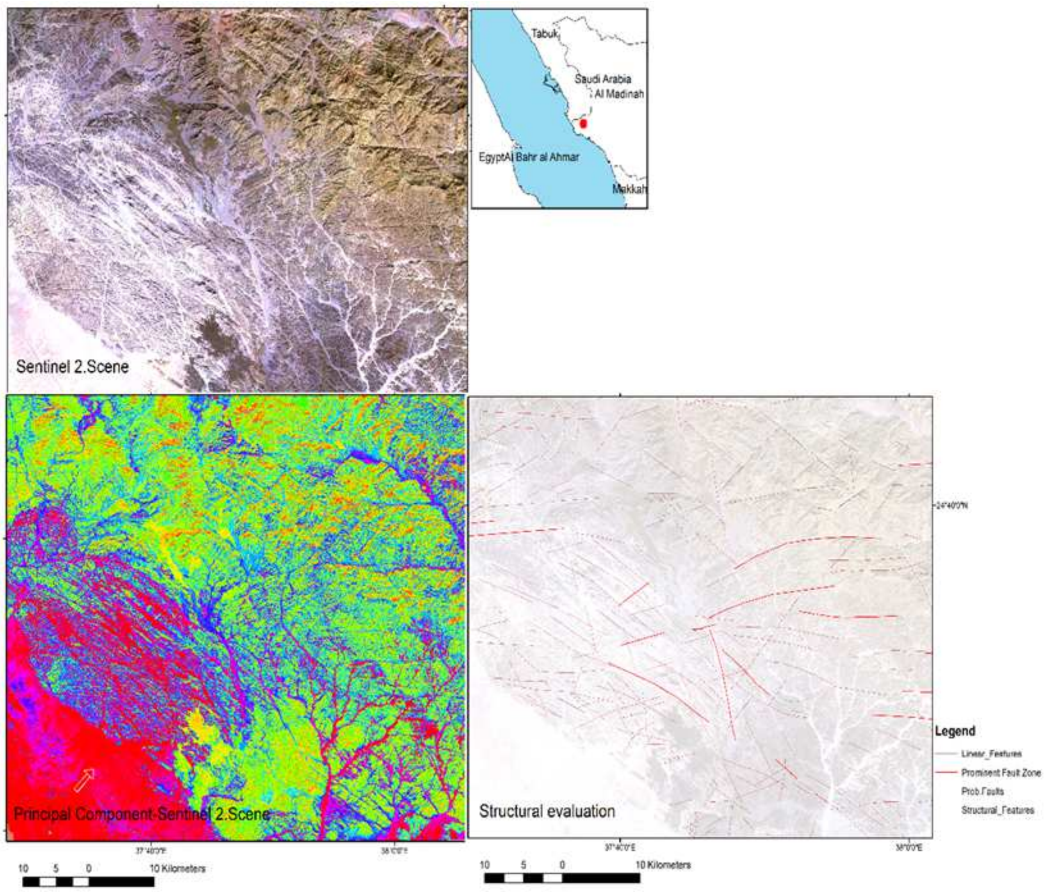

Figure 8. Traces of compression visible as parallel, NW-SE- oriented linear features (black arrows), perpendicular to the direction of the main stress

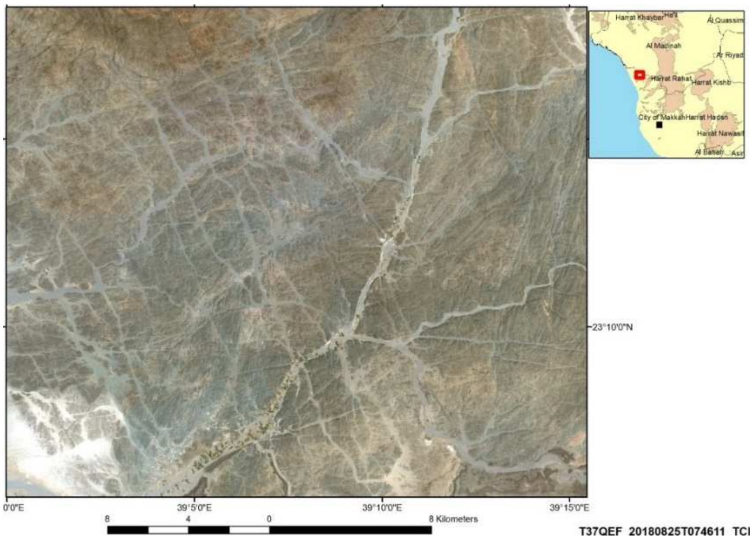

Figure 9. Traces of compression visible on a Sentinel 2 scene

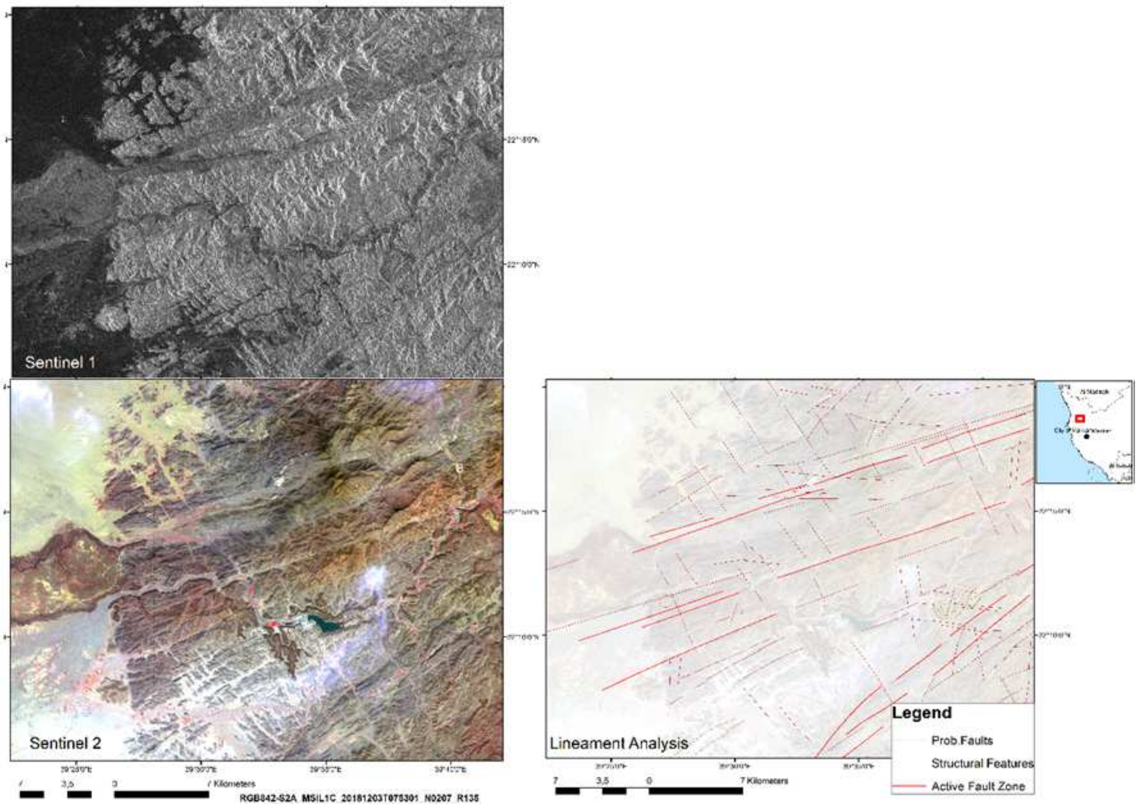

Figure 10. Traces of compression visible on Sentinel 1 radar and Sentinel 2 optical images as NW-SE oriented parallel, linear features

The first step used the "Fillsink" algorithm from the ArcMap software package that identifies the point or set of adjacent points surrounded by neighbors with higher elevation and rises to the lowest value on the depressions boundary. This procedure then fills all depressions in the DEM, including both those generated from data errors (spurious artifacts) and those that record real topographic features.

The second step was to extract the sink depths in these areas by differencing the maps between the sink-filled ("depressionless" DEM) and original DEM. The difference image highlight the different depressions [25]. This approach was carried out based on SRTM, Aster and ALOS PALSAR DEM data, comparing the results. When evaluating the DEM difference maps of all the three DEM data sets, a linear, parallel arrangement of the sinks becomes visible, oriented parallel to the coast, even in the youngest sediments (Figures 11,12). The origin of this parallel, linear arrangement might be complex and has to be discussed and to be further investigated: Reasons among others might be a) compression of the subsurface, b) traces of uplift, c) traces of parallel longitudinal dunes underneath the younger eolian covers, linear wind erosion, and flash flood sediments? Due to the rifting processes in the Red Sea and the movements of the Arabian Plate towards NE with velocities of about 10 to 15 mm / year [8] it seems most likely that the parallel alignment of linear features is related to compression.

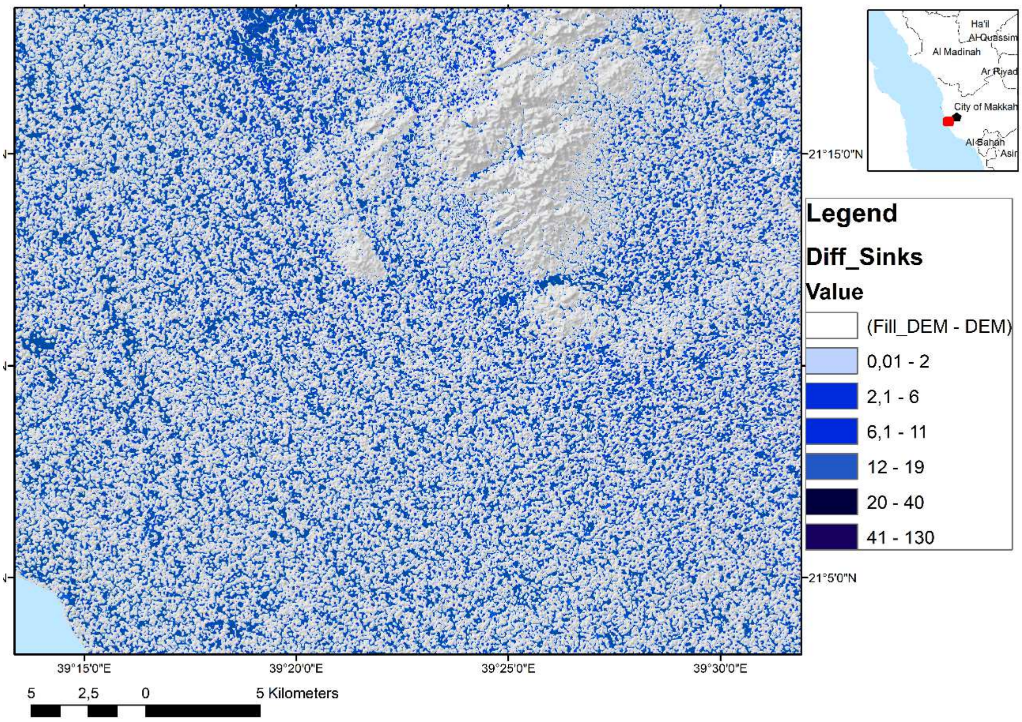

Figure 11. Difference DEM map of the coastal area of Jeddah showing a linear, NW-SE oriented, parallel arrangement of the "sinks" in the SRTM-DEM

When comparing the position of earthquake epicentres with the lineament map of W-Saudi Arabia, it appears, that the earthquake epicenters occur concentrated along these SW-NE striking shear zones (Figures 1,2). Whether these earthquakes were triggered by stress accumulations along fault zones or by magmatic activity in the subsurface, or the combination of both, has still to be investigated more detailed in the affected areas. In the scope of this research the monitoring of those zones of weakness is important regarding the safety of infrastructure. The relatively youngest, prominent fault zones cutting even through Holocene sediments, striking N-S, are visible on the different satellite data as linear, tonal anomalies.

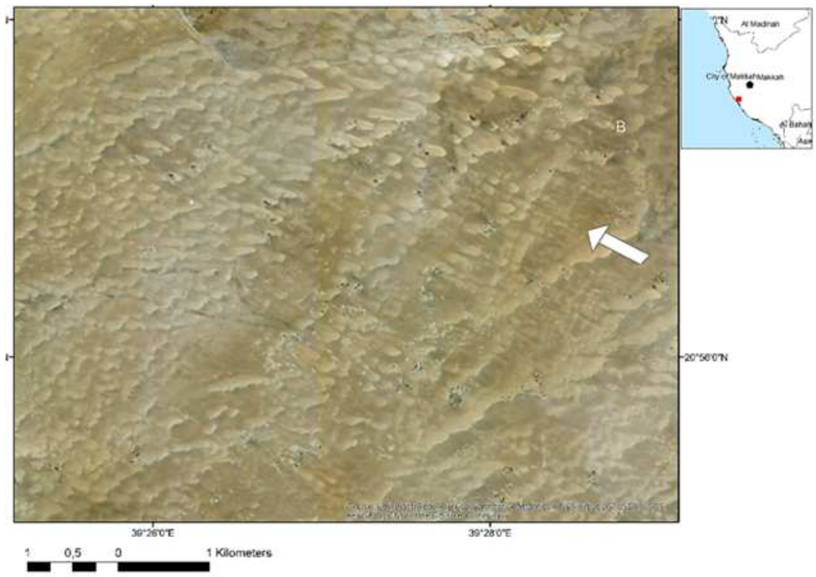

Figure 12. Parallel, linear, NW-SE oriented features within coastal dune fields

4.4. Contribution of the GIS integrated evaluation of satellite data to the monitoring of volcanic features

After digital image processing of Sentinel 2, Landsat 8, ASTER and OrbView data the use of satellite data for volcanic monitoring becomes evident: Remote sensing and GIS can contribute to

- the mapping of volcanic cinder cones,
- the mapping of visible fault zones and dikes in the area of cinder cone fields,
- the mapping of the most recent lava flow,
- the detection of traces of age differences and types of volcanic features based on erosional and weathering conditions and on the lithologic composition.

A systematic inventory and mapping of cinder cones and youngest volcanic eruptions in the different volcanic areas was carried out, combined with a structural (lineament) analysis (Figure 13).

Digital image processing tools in ENVI, SNAP and ArcGIS software help to identify cinder cones by RGB band combinations and Gaussian filters or Principal Component analysis. About 2500 cinder cones were digitized. The size of the cinder cones is relatively constant about 200 to more than 1000 m in diameter (Figure 14). The mapping of the relatively youngest traces of volcanic activity such as dyke intrusions or most recent lava outbreak provides information of fault zones that are susceptible to magmatic up rise. Such information are important for the understanding, where and when future eruptions may occur. This might be important for hazard preparedness. Thus, the structural evaluation of the different satellite data is used to identify those fault zones that are obviously related to magma ascent. The strike and type of those fault zones changes from north to south. Whereas in the northern part mainly NW-SE oriented fault zones are dominant, in the central part of western Saudi Arabia NNW-SSE, and N-S striking fault zones are prevailing (Figure 7). The concentration of volcanic cones along the NNW-SSE oriented Madinah-Makkah volcanic line is clearly visible [32]. In the southern part NE-SW oriented fault zones are influencing the volcanic pattern as in Harrat Nawasif. Special attention is directed to the intersection of larger fault zones. Whenever prominent SW-NE striking fault zones are crossing N-S-oriented ones in the Harrat areas, a concentration of cinder cones align along the fault zones in the intersections can be observed.

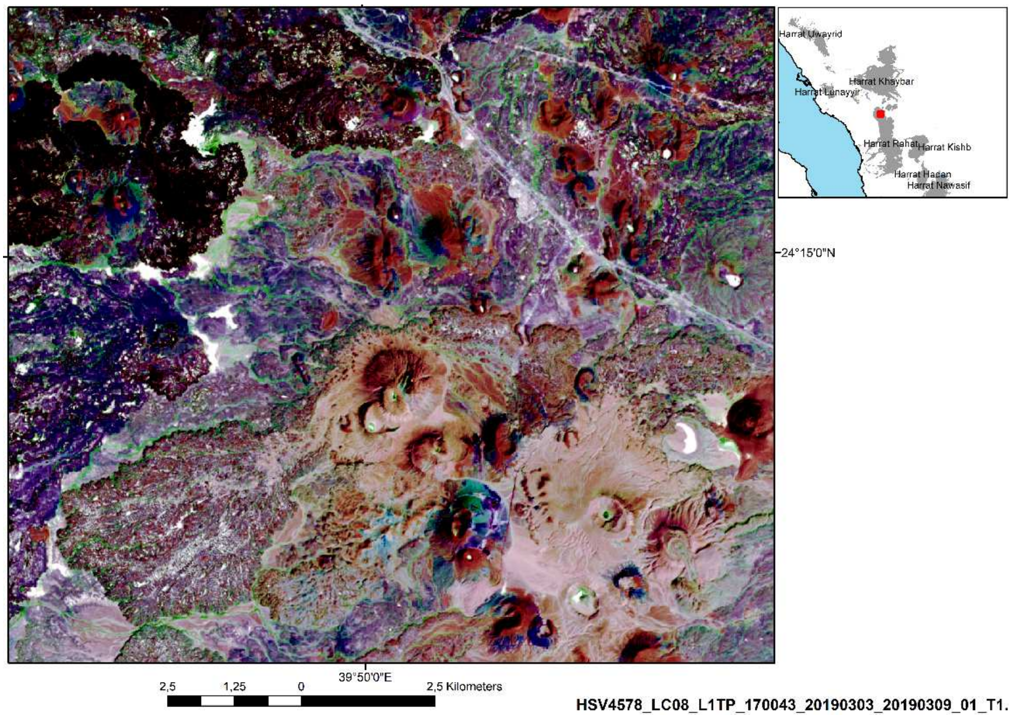

Figure 13. Cinder cones of alkali-olivine basalt [19] (red) aligned along N-S and SW-NE oriented fault zones and recent lava outbreak areas with thin fluid basalt lava flows in the north of Harrat Rahat visible on a Landsat 8 scene

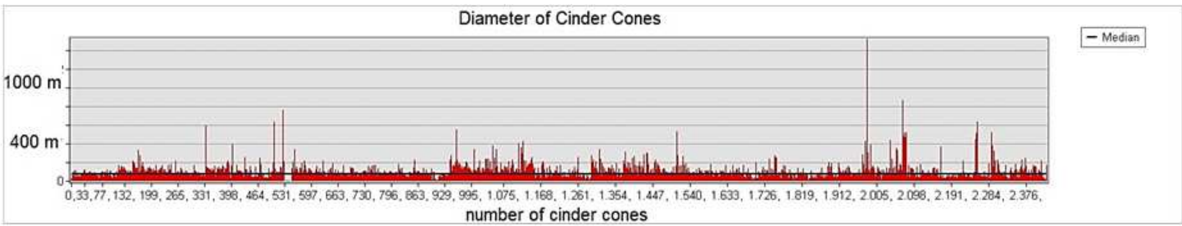

Figure 14. Size of cinder cones (based on about 2500 mapped cinder cones) in W-Saudi Arabia

The question arises, why the volcanic activity of Harrat Rahat has stopped in the N of the City of Mecca? The volcanic activity of the Madinah-Makkah zone (comprising the area along the NNW-SSE axis of Harrat Rahat) almost stops along the SW-NE oriented Wadi Fatima shear zone (Figure 7). Lava fields and cinder cones occur as if shifted towards east in the area of Harrat Hadan and Harrat Nawasif. As one of the explanations for this phenomenon might be discussed the occurrence of ring structures: When analysing the position of circular structures and the outcrop of lava, it seems as if the circular structures have an influence on the occurrence and shape of lava flow. Obviously larger, compact intrusive bodies are forming a hindrance for uprising, larger, volcanic intrusions. In areas with a higher density of large circular structures such as in the area of Makkah younger lava sheets and cinder cones could not be observed. However, the larger ring structures are often intersected by dykes.

The following Sentinel-2 scenes (Figures 15, 16, 17) show circular features that are partly surrounded by younger lava sheets. Whether this is caused only by topographic reasons as some ring structures are forming domes causing a flowing around, or / and selective erosion or by circular structures hindering recent magmatic ascent and flow, this has still to be investigated in the specific cases.

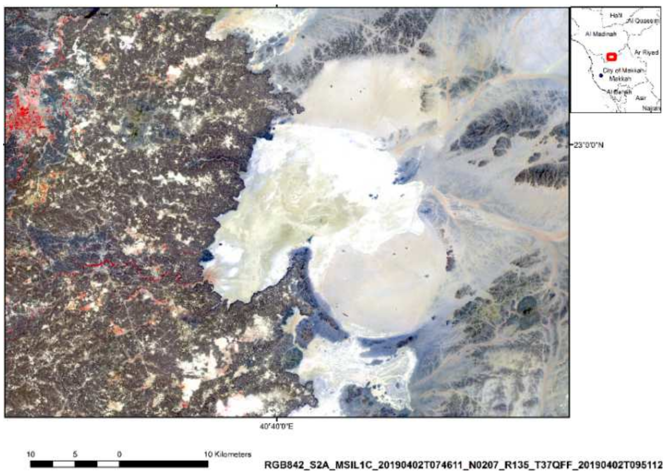

Figure 15. Sentinel 2-scene (RGB: Bands 8,4,2) showing ring structures in the east of Harrat Rahat surrounded by lava in the western part

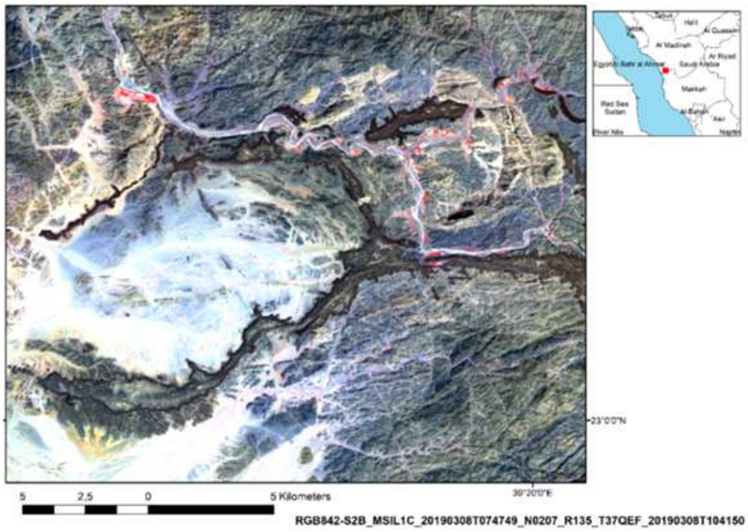

Figure 16. Lava flow around oval (left) and circular (upper right) shaped structures

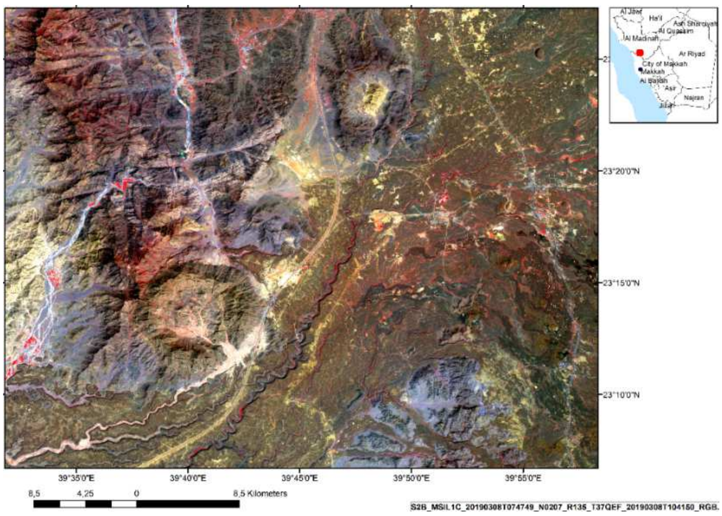

Figure 17. Lava sheets surrounding ring structures

Based on evaluations of satellite data it is possible to categorize the different volcanic features in W-Saudi Arabia systematically based on the geomorphologic properties, erosional and weathering conditions and on the lithologic composition: cinder cones with latest lava outbreak, intact lava sheets, dissolved and intersected lava sheets and lava inselbergs, lava fields with developed drainage system, and isolated volcanic features intersecting eolian and fluvial sediments. Dissolved lava sheets and inselbergs occur predominantly at the western part of the Harrats, whereas the lava sheets in the eastern part are characterized by the development of a dense drainage pattern and small depressions filled with evaporitic and youngest sedimentary covers.

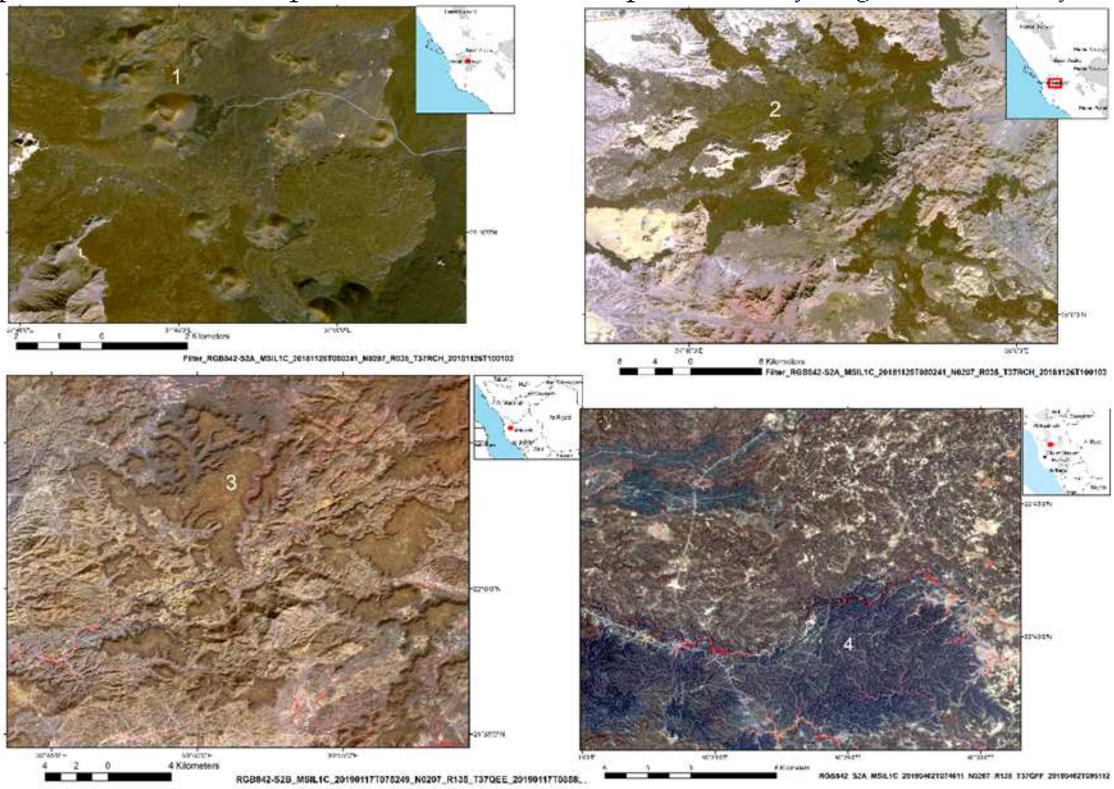

Figure 18. Geomorphologic types of volcanic features
1- cinder cones, 2 – lava outbreak with high lava viscosity, 3 – lava inselbergs, 4 – eroded lava sheets with drainage patterns

4.5. Contribution of remote sensing and GIS to the detection of factors influencing tsunami hazard

The input of remote sensing and GIS can be considered only as a small part of the whole "mosaic" of tsunami research approaches. Nevertheless, it offers a low-cost to no-cost approach, that can be used in any area, providing a first basic data stock for emergency preparedness by providing for example susceptibility-to-flooding maps. Summarizing factors influencing flooding susceptibility such as relatively low height levels (<10 m) help to detect areas with higher flooding susceptibility. Those areas might be prone to flooding in case of a severe tsunami event. The following Fig.19 a and b shows an example of the city of Jeddah, intersecting road-shapefiles with height levels below 5 m, assuming a tsunami wave-height of 5 meters as the leading parameter for tsunami preparedness. In case of high energetic flood waves from the Red Sea or in case of flash floods these road segments < 5m might be prone first to flooding due to their lowest height level.

The source of tsunamis, the direction of the incoming waves, their height and energy cannot yet predicted. However, when analysing the influence of the coastal morphology on the streaming pattern in relation to wind and wave directions, it supports a better understanding of what might happen in case of high energetic flood waves. Given that coastal flow is the product of a complex mix of factors (i.e. freshwater discharge, tides, temperature, salinity, winds in various frequency bands and the influence of motions imposed from seiche movements), coastal dynamics may be regarded almost as regional. The tide amplitude at the time of a potential tsunami directly affects the inundation height as well and, hence, the impact of the tsunami on the coastal areas. Even in the case of small amplitude tsunamis, the combination of the tsunami with a higher tide might result in a higher wave height.

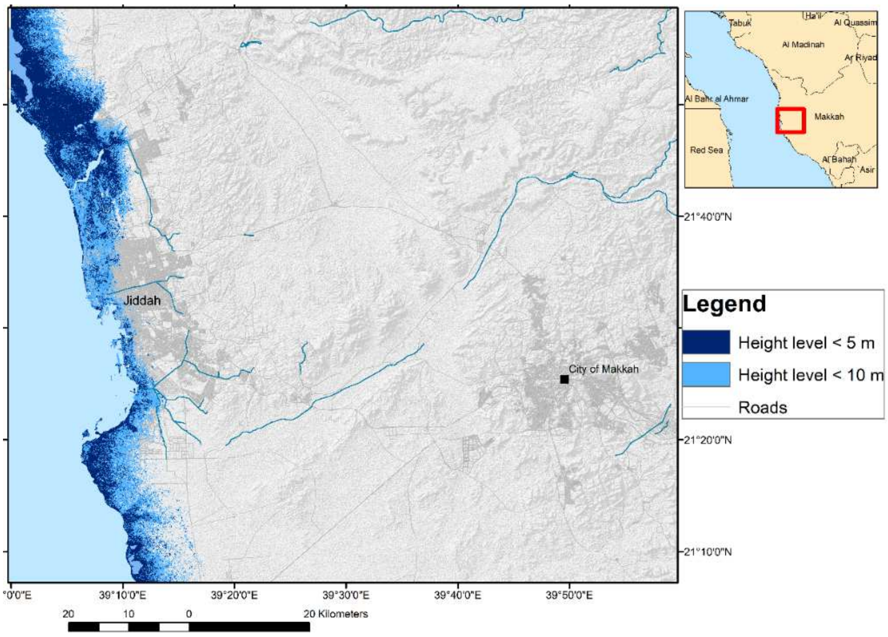

Figure 19 a. Height levels below 10 m calculated based on SRTM DEM data (30 m resolution)

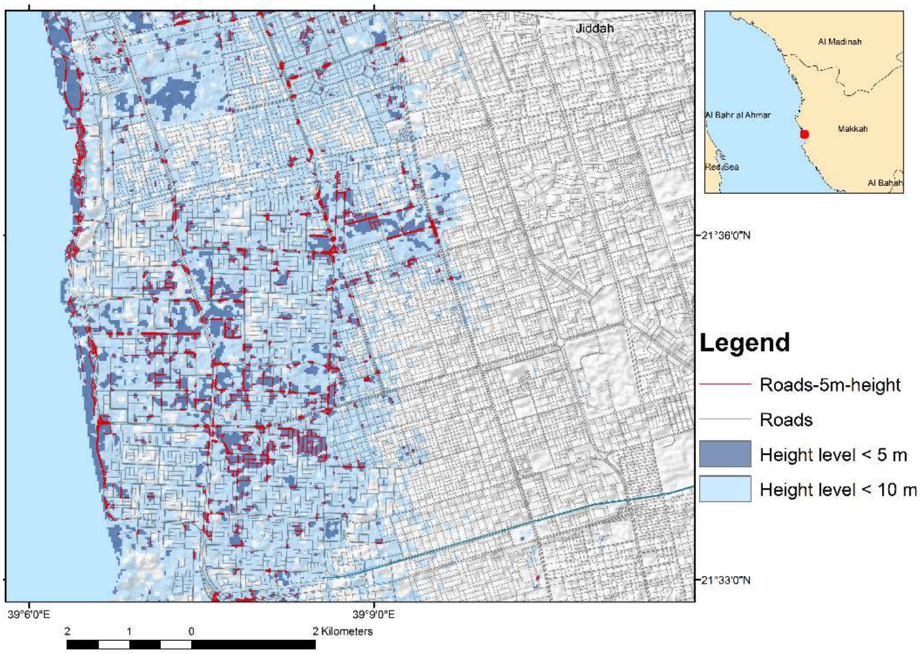

Figure 19 b. Road segments below 5 m height level (red) in Jeddah calculated based on ALOS PALSAR DEM data (12.5 m resolution)

Satellite scenes reveal streaming pattern of the upper cm of the water surface. After digital image processing and enhancement especially of the thermal LANDSAT and ASTER bands from the coastal areas, water currents at the acquisition time become clearly visible. Of course, these images reflect the water, wind and temperature conditions at the data acquisition time. However, the streaming pattern visible on the LANDSAT imageries provides some useful information of the influence of coastal morphology on water currents, that might be of interest for the better understanding of storm surge, meteo-tsunamis and tsunami wave propagation and their interaction with the coastal morphologic properties.

Time series of LANDSAT imageries form an important input for this research, as they contribute to a better understanding of the streaming pattern among different conditions such as wind directions and intensities or seasonal temperature and salinity changes. The next figure (Figure 20) demonstrates Landsat 8-senes (RGB band combination 2,1,7) of different acquisition times with different wind and streaming conditions. Islands in front of the coast line are influencing and modifying the wave patterns, their density and sizes (Figures 20,21), often causing turbulent flow. Depending on the wind direction waves are interfering each other within the area of the islands. The islands situated in front of the coast line might slow down high energetic flood waves directed towards the coast.

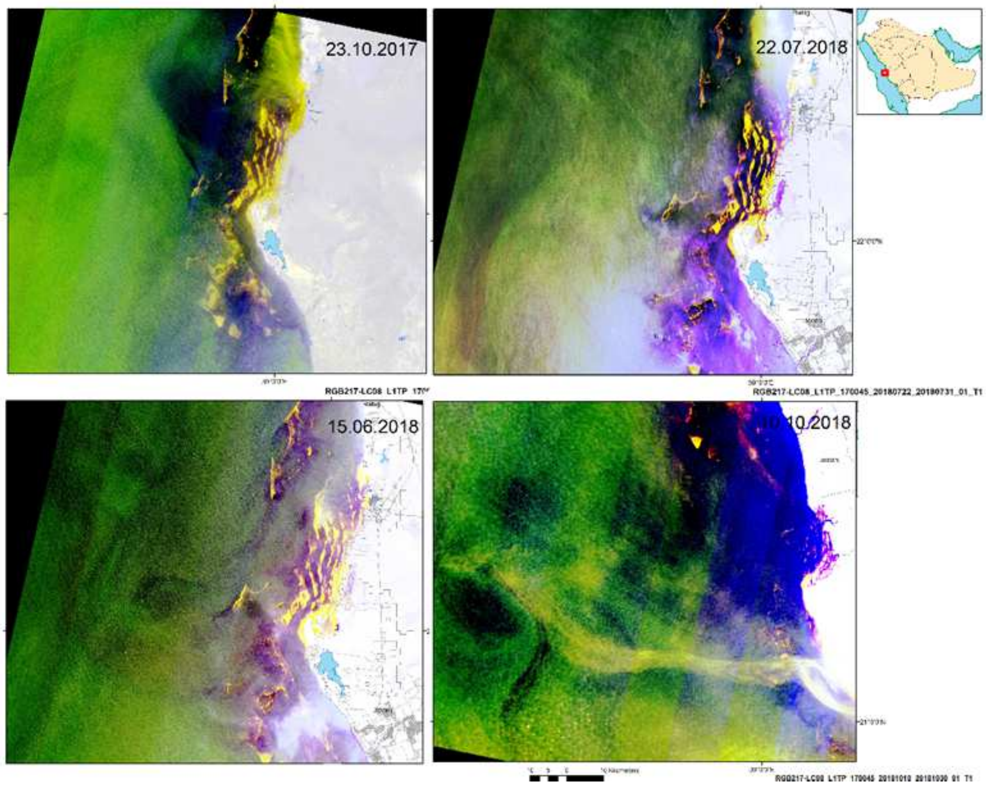

Figure 20. Different streaming and wave patterns at the coast of Jiddah visible on Landsat 8-scenes (RGB, Bands 2,1,7) On the scene of 10.10.2018 the sediment input of a dust storm is visible as yellow band.

The bathymetric situation has an influence on the streaming pattern as well. Figure 21 visualizes the bathymetric contour lines on the Landsat 8-scene and, thus, showing the difference in the streaming pattern visible on the satellite image from deeper areas to flat shelf areas.

When analysing the coastal morphology and GEBCO bathymetric data deeper, submarine valleys /canyons can be observed that are partly oriented perpendicular towards the coast (white arrows in Figure 22). In case of high energetic flood waves such as tsunami waves caused by earthquakes, volcanic eruptions or submarine mass movements in the Red Sea the tsunami wave energies might be focused and concentrated along these valleys and, thus, in this case increasing the flooding extent in those coast segments.

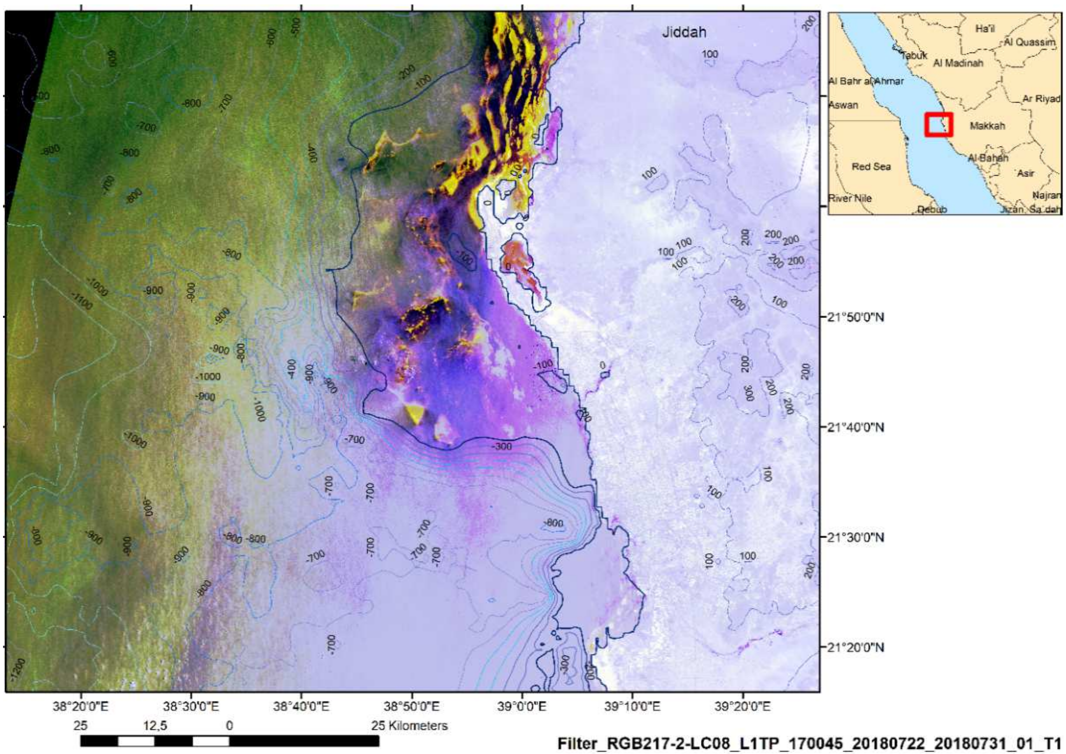

Figure 21. Submarine topography and islands influencing the streaming pattern near Jeddah

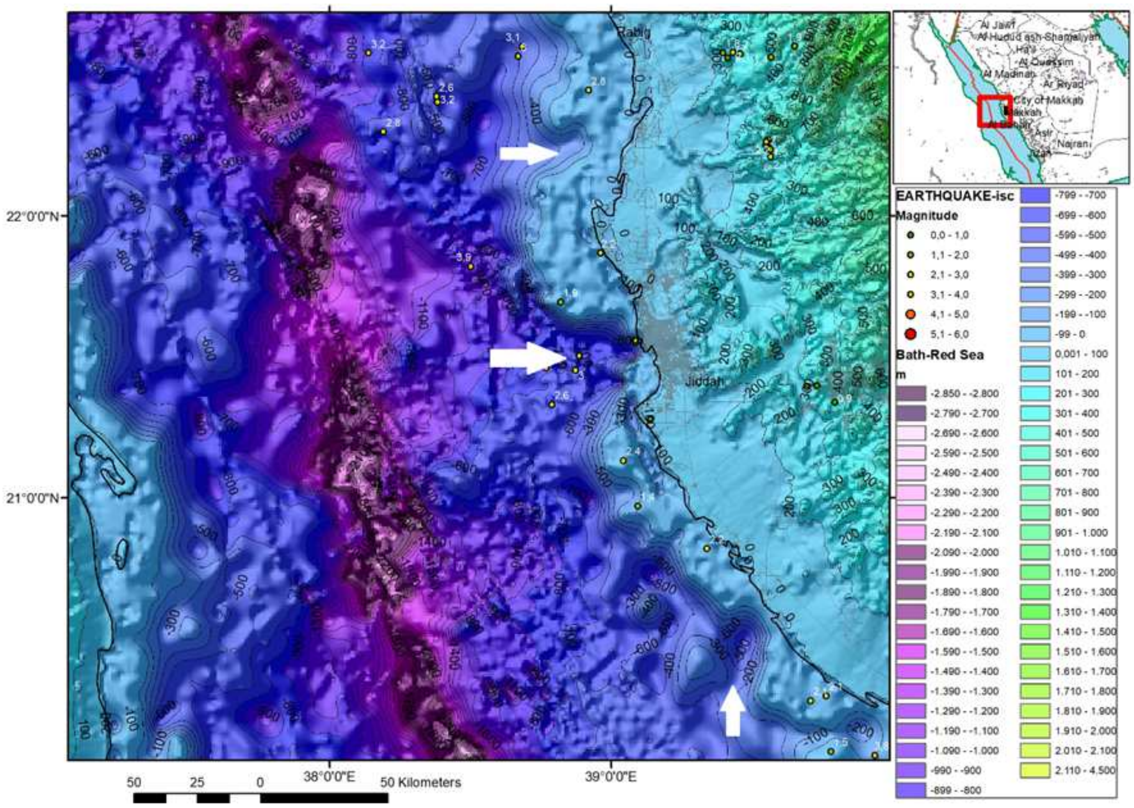

Figure 22. Submarine valleys near the coast with potential focus of high energetic flood waves such as tsunami waves. The map was created based on GEBCO bathymetric data.

5. Discussion

The examples of the use of remote sensing and GIS tools for the monitoring of natural hazards have shown that the continuously, systematic documentation and surveillance based on satellite data is a prerequisite not only for emergency preparedness, but also for the preparation of effective field work. Observations such as of geologic features like traces of compression or ring structures need further investigations. The evaluation of the satellite data helps to focus this research. For example: The analysis of the different satellite data allows the detection of structural features in the subsurface such as faults and ring structures more detailed than represented so far in geologic maps or even not visible in the field due to younger sedimentary covers. Their specific origin and tectonic role should be investigated.

Landsat and Sentinel 1 and 2-data are an important tool for the water streaming observation in the Red Sea. When carried out in a regular pattern (of course combined with available in situ measurements), remote sensing data help to get more detailed knowledge about the complex factors influencing the currents in the Red Sea. This input will be important when dealing with storm surge or tsunami events.

6. Conclusions

The combination of the evaluation results based on satellite images and digital elevation data proved to be effective as an input for geo-hazard assessment. Prevention of damage related to natural hazards (such as extreme rainfall or earthquakes and resulting secondary effects) to human life and infrastructure requires preparedness and mitigation measurements that should be based on a regularly updated, GIS integrated data mining in order to create a data bank for the different geohazards. The frequent coverage of regularly available data such as Sentinel and Landsat are fundamental for the monitoring of the natural hazards in western Saudi Arabia.

Evaluations of the different satellite data from W-Saudi Arabia contribute to the identification of areas prone to geohazards, to the detection of the different types of hazards and of some of the causal factors influencing the disposition to the specific hazards. More detailed and partly new knowledge could be derived from the structural analysis of the remote sensing data.

Author Contributions: Conceptualization, Theilen-Willige.; methodology, Theilen-Willige.; software, Theilen-Willige.; validation, Theilen-Willige and Wenzel.; formal analysis, Theilen-Willige and Wenzel.; investigation, Theilen-Willige.; resources, Theilen-Willige and Wenzel; writing—original draft preparation, Theilen-Willige .; writing—review and editing, Theilen-Willige. ; visualization, Theilen-Willige.; supervision, Wenzel.; project administration, Helmut Wenzel.; funding acquisition, Helmut Wenzel.

Acknowledgments: The authors are grateful for the input of the reviewers.

Conflicts of Interest:

"The authors declare no conflict of interest."

References

1. Al-Bassam,A.M.; Zaidi,F.K.; Hussein,M.T. Natural hazards in Saudi Arabia. In: Extreme Natural Hazards, Disaster Risks and Societal Implications. Eds. Ismail-Zadeh,A.; Urrutia-Fucugauchi,J.; Kijko,A.; Zaliapin,I.. Published by *Cambridge University Press*, 2014, pp. 243-251, Comp. by: K.Venkatesan, Stage: Proof Chapter No.: 18. Available online: https://fac.ksu.edu.sa/sites/default/files/enhans.pdf (accessed on 14.10.2018)
2. Centre for Research on the Epidemiology of Disasters (CRED). EM-DAT Database. Available online: https://www.emdat.be/database (accessed on 03.06.2018).
3. Saudi Geological Survey (SGS), National Centre for and Volcanoes, Earthquake Seismology: Tectonics of the Arabian Plate. Available online: https://www.sgs.org.sa/English/Mobile/NaturalHazards/pages/geohazard.aspx (accessed on 25.10.2018).
4. Intergovernmental Panel on Climate Change (IPCC). IPCC Fifth Assessment Report (AR5), Observed Climate Change Impacts Database, Version 2.01. Palisades, NY: NASA Socioeconomic Data and Applications Center (SEDAC). 2017. Available online: https://doi.org/10.7927/H4FT8J0 (accessed on 03.10.2018).

5. Youssef,A.M.; Maerz,N,H. Overview of some geological hazards in the Saudi Arabia. *Environ Earth Sci,* 2013, 70, 3115–3130, DOI 10.1007/s12665-013-2373-4
6. Al-Ghamdi,K.; Elzahrany,R.A.; Mirza,M.N.; Gomaa M. Dawod,G.M. Impacts of urban growth on flood hazards in Makkah City, Saudi Arabia. *International Journal of Water Resources and Environmental Engineering*, 2012, Vol. 4(2), pp. 23-34, DOI: 10.5897/IJWREE11.128
7. Adams, R.D.; Barazangi, M. Seismotectonics And Seismology. In: The Arab Region, A Brief Summary And Future Plans. *Bulletin Of The Seismological Society Of America*, 1984, Vol.74, pp.1011-1030.
8. Sakr,K;, Abdel-Monem,S.M.; Khalil,H.; Mahmoud,S.; Hamimi,Z.; Al-Aydrus,A.; Al Subary,A.; Al-Kottbah,A.; El Ganad,I.; Al-Gabary,A.;Al-Wosabi,M.A. A Study of Crustal Deformation along the Red Sea Region using Geodetic and Seismic Data from Egypt and Yemen. *Acta Geophysica Polonica* , 2005,Vol. 53, No. 1, pp.75-85.
9. Ligi,M.; Bonatti,E.; Tontini,F.C.; Cipriani,A.; Cocchi,L.; Schettino,A.; Bortoluzzi,G.; Ferrante,V.; Khalil,S.; Mitchel, N.C.; Rasul,N. Initial burst of oceanic crust accretion in the Red Sea due to edge driven mantle convection. *GEOLOGY*, November 2011, vol.39, no. 11; pp. 1019–1022; DOI:10.1130/G32243.1
10. Kassema, O. M. K.; Hamimi,Z. Finite Strain Analysis of the Wadi Fatima Shear Zone in Western Arabia, Saudi Arabia. *Geotectonics*,2018, Vol.52, 2, pp.251–265. DOI: 10.1134/S0016852118020036, Available online:https://www.researchgate.net/publication/327944832_Finite_Strain_Analysis_of_the_Wadi_Fatima_Shear_Zone_in_Western_Arabia_Saudi_Arabia_1
11. El-Isa,Z.H.; Al Shanti,A. Seismicity and tectonics of the Red Sea and western Arabia. *Geophysical Journal International*, 1989, Vol. 97, 3, pp. 449–457, Available online: https://doi.org/10.1111/j.1365-246X.1989.tb00515.x
12. USGS US Geological Survey (USGS), Availabele online: https://earthquake.usgs.gov/earthquakes/search/ (accessed on 12.10.2018)
13. International Seismological Centre (ISC), *On-line Bulletin*, http://www.isc.ac.uk, International Seismol. Cent., Thatcham, United Kingdom, 2018, http://doi.org/10.31905/D808B830
14. European-Mediterranean Seismological Centre (EMSC): https://www.emsc-csem.org/#2
15. Smithsonian Institution's Global Volcanism Program (GVP) , 2016. Eruptions, Earthquakes & Emissions, v. 1.0 (internet application). Smithsonian Institution, Available online: https://volcano.si.edu/E3/). (Accessed 25.01.2019)
16. Moufti,M.R., Nemeth,K., Murci,H.,and Lindsay,J.M. (2013): The 1256 AD Al Madinah historic eruption geosite as the youngest volcanic chain in the Kingdom of Saudi Arabia. *Int J Earth Sci (Geol Rundsch),* 102:1069–1070, DOI 10.1007/s00531-013-0878-4
17. Pallister,J.S.; McCausland,W.A.; Jónsson,S.; Lu,Z.; Zahran,H.M.; El Hadidy,S.; Aburukbah,A.; Stewart,I.C.F.; Lundgren,P.R.; White,R.A.; Moufti,M.R. Broad accommodation of rift-related extension recorded by dyke intrusion in Saudi Arabia. *Nature Geoscience*, 2010, Vol. 3, pp.705-712. DOI: 10.1038/NGEO966
18. Xu,W.; Jónsson,S.; Corbi,F ; Rivalta,E. Graben formation and dike arrest during the 2009 Harrat Lunayyir dike intrusion in Saudi Arabia: Insights from InSAR, stress calculations and analog experiments. *J. Geophys. Res. Solid Earth*, 121,pp. 2837-2851. DOI:10.1002/2015JB012505.
19. Camp,V.E.; Hooper,P.R.; Roobol,M.J.; White,D.L. The Madinah eruption, Saudi Arabia: Magma mixing and simultaneous extrusion of three basaltic chemical types. *Bulletin of Volcanology*, 1987,pp. 49:489-508. DOI: 10.1007/BF01245475
20. Jordan,B.R. Tsunamis of the Arabian Peninsula - A Guide of Historic Events. *Science of Tsunami Hazards*, 2008, Vol. 27, 1, pp.31-46.
21. National Oceanic and Atmospheric Administration (NOAA), Global Historical Tsunami Database, doi:10.7289/V5PN93H7, https://www.ngdc.noaa.gov/hazard/tsu_db.shtml
22. General Bathymetric Chart of the Oceans (GEBCO), GEBCO's gridded bathymetric data set, https://www.gebco.net/data_and_products/gridded_bathymetry_data/
23. NOAA, https://oceanservice.noaa.gov/facts/seiche.html
24. Theilen-Willige (2015,) [24] Theilen-Willige, B., Charif, A., Chaïbi, M., Ait Malek, H. Flash Floods in the Guelmim Area / SW-Morocco - Use of Remote Sensing and GIS-Tools for the Detection of Flooding Prone Areas. *Geosciences* 2015, 5(2), 203-221; doi:10.3390/geosciences5020203, http://www.mdpi.com/2076-3263/5/2/203

25. Theilen-Willige B., Savvaidis,P., Tziavos,I.N., Papadopoulou,I. (2012): Remote Sensing and Geographic Information Systems (GIS) Contribution to the Inventory of Infrastructure Susceptible to Earthquake and Flooding Hazards in North-Eastern Greece. *Geosciences* 2012, 2(4), 203-220; https://doi.org/10.3390/geosciences2040203
26. USGS, EarthExplorer, https://earthexplorer.usgs.gov/
27. Alaska Satellite Facility (ASF), JAXA/METI, accessed through ASF DAAC, https://www.asf.alaska.edu/
28. OpenStreetMap Data Extracts. Available online:: http://download.geofabrik.de/ (accessed on 25.09.2018)
29. Fnais, M.; Amri, A. A.; Abdelrahman, K.; Abdelmonem,E.; El-Hady,S.. Seismicity and Seismotectonics of Jeddah-Makkah Region, West-Central Saudi Arabia. *Journal of Earth Science*, 2015, 26,5, pp. 746–754. doi: 10.1007/s12583-015-0587-y
30. ArRajehi,A.; McClusky,S.; Reilinger,R.; Daoud,M.; Alchalbi,A.; Ergintav,S.; Gomez,F.; Sholan,J.; Bou-Rabee,F.; Ogubazghi,G,; Haileab,B.; Fisseha,S.; Asfaw,L.; Mahmoud,S.; Rayan,A.; Bendik,R.; Kogan,L. Geodetic constraints on present-day motion of the Arabian Plate: Implications for Red Sea and Gulf of Aden rifting. *TECTONICS*, 2010, Vol. 29, TC3011, doi:10.1029/2009TC002482
31. Hamimi,Z.; Matsah,M.; El-Shafei,M.; El-Fakharani,A.; Shujoon,A.; Al-Gabali,M. Wadi Fatima Thin-Skinned Foreland FAT Belt: A Post Amalgamation Marine Basin in the Arabian Shield. *Open Journal of Geology*, 2012, 2, pp. 271-293.
32. Downs,D.T.; Stelten,M.E.; Champion,D.E.; DietterichH.R.; Nawab,Z.; Zahran,H.; Hassan,K.; Shawali,J. Volcanic history of the northernmost part of the Harrat Rahat volcanic field, Saudi Arabia. *Geosphere*, 2018, vol. 14, 3, pp. 1253–1282. doi:10.1130/GES01625.1